Science of Remote Sensing 9 (2024) 100116

Contents lists available at ScienceDirect

Science of Remote Sensing

journal homepage: www.sciencedirect.com/journal/science-of-remote-sensing

The apparent effect of orbital drift on time series of MODIS MOD10A1 albedo on the Greenland ice sheet

Shunan Feng [a,*], Adrien Wehrlé [b], Joseph Mitchell Cook [a], Alexandre Magno Anesio [a], Jason Eric Box [c], Liane G. Benning [d,e], Martyn Tranter [a,**]

[a] Department of Environmental Sciences, Aarhus University, Frederiksborgvej 399, Roskilde, DK-4000, Denmark
[b] Institute of Geography, University of Zurich, Zurich, 8052, Switzerland
[c] Geological Survey of Denmark and Greenland, Copenhagen, Denmark
[d] GFZ German Research Centre for Geosciences, Section Interface Geochemistry, Telegrafenberg, Potsdam, 14473, Germany
[e] Department of Earth Sciences, Free University of Berlin, Berlin, 12249, Germany

ARTICLE INFO

Keywords:
Orbit drift
MODIS
Albedo
Greenland ice sheet
Time series
Google Earth Engine

ABSTRACT

The NASA MODIS MOD10A1 snow albedo product has enabled numerous glaciological applications. The temporal consistency of MODIS albedo is critical to obtaining reliable results from this 22-year time series. The orbit of Terra began to drift toward earlier acquisition times after the final inclination adjustment maneuver to maintain its nominal orbit by NASA on 27 February 2020, which may introduce biases that compromise the accuracy of quantitative time series analysis as the drift continues. Here, we evaluate the impact of Terra's orbital drift by comparing the differences between the Terra MODIS albedo and albedo products derived from Aqua MODIS, harmonized Landsat and Sentinel 2, Sentinel 3, and PROMICE (Programme for Monitoring of the Greenland Ice Sheet) ground measurements over the Greenland ice sheet. Our results suggest that the influence of orbital drift on albedo is small (+0.01 in 2020), but potentially biased for time series analysis. Our analysis also finds that the drift effect that causes earlier image acquisition time may lead to more apparently cloudy pixels and thus effectively reduce the Terra MODIS temporal resolution over Greenland.

1. Introduction

Surface albedo controls the absorption of solar energy, and is a key factor governing surface melt and runoff in polar and other glaciated areas (Stroeve et al., 2006; Box et al., 2012; Naegeli et al., 2017, 2019). Albedo products derived from satellite remote sensing data provide valuable time series data for different environments around the globe, including the cryosphere. The MODerate resolution Imaging Spectroradiometer (MODIS) sensors aboard the two sun-synchronous orbit satellites, Terra (launched on 18 Dec. 1999) and Aqua (launched on 4 May 2002), have provided more than two decades of near daily global earth observatory records (Barnes et al., 2003; Giglio and Roy, 2022). Both MODIS sensors have been in operation well beyond their designated six-year operational life expectancy (Xiong et al., 2015). The MODIS Snow Albedo Daily Tile is produced by applying an algorithm (Klein and Stroeve, 2002) to both Terra MODIS and Aqua MODIS, and forms part of the Snow Cover Daily Global 500 m (MOD10A1 for Terra and MYD10A1 for Aqua) product (Hall et al., 1995, 2018; Hall and Riggs, 2007), distributed by the US National Snow and Ice Data Center (NSIDC). The MODIS daily snow and ice albedo products have been validated with *in situ* measurements, e.g., Liang (2005); Stroeve et al. (2006); Hall and Riggs (2007); Box et al. (2017); Casey et al. (2017), and reprocessed to improve the data quality (Schaaf et al., 2011a; Hall et al., 2018). Their consistency has been repeatedly checked (Stroeve et al., 2013; Polashenski et al., 2015; Casey et al., 2017). MODIS albedo has been widely used in glaciological applications, such as estimating snow cover duration (Dietz et al., 2015), land ice mass balance (Østby et al., 2017; Xiao et al., 2022), snowline variations (Ryan et al., 2019; Noël et al., 2019), accumulation area ratio (Box et al., 2022), and meltwater runoff modeling e.g., van As et al. (2017); Cook et al. (2020). MODIS albedo is also commonly used as a reference product in validating modeled and/or measured albedo products (Alexander et al., 2014; Macander et al., 2015; Kokhanovsky et al., 2020).

Greenland ice sheet surface melt is enhanced by snowcover ablation,

* Corresponding author.
** Corresponding author.
E-mail address: shunan.feng@envs.au.dk (S. Feng).

https://doi.org/10.1016/j.srs.2023.100116
Received 15 June 2023; Received in revised form 7 December 2023; Accepted 16 December 2023
Available online 20 December 2023

exposing a relatively dark, low albedo ablation area. The ablation or melt area of the ice sheet contributes over 80% of the total runoff (Steger et al., 2017; Irvine-Fynn et al., 2021) and the darkening of the bare ice area has been enhancing melting (Van As et al., 2013; Shimada et al., 2016; Cook et al., 2017; Ryan et al., 2018). Accurate discrimination between artifacts and real surface process changes (e.g., the darkening of the ice sheet) is important in interpreting long time series of remote sensing products (Roy et al., 2002; Tian et al., 2015; Hall et al., 2018; Giglio and Roy, 2022). The decline in ice sheet albedo derived from MODIS data has ranged from -0.060 · decade^{-1} to -0.028 · decade^{-1} (Box et al., 2012; He et al., 2013; Alexander et al., 2014), depending on the period being considered. The long term darkening trend may be prone to error if a bias in the data acquisition is of similar magnitude to or of greater magnitude than the real trend. Bias may arise from changes in the satellite sampling time due to orbital drifts.

Orbital drift impacts the consistency of time series of satellite data, e.g., the advanced very high resolution radiometers (AVHRR) (Kaufmann et al., 2000; Sobrino et al., 2008), Landsat 5 (Zhang and Roy, 2016; Roy et al., 2020), and Landsat 7 (Qiu et al., 2021), from different aspects. Those aspects include 1) the local acquisition time, 2) the Bidirectional Reflectance Distribution Function (BRDF) effect, 3) cloudiness, and 4) the effective spatial resolution. Orbital drift has occurred at different operational stages of Terra and Aqua (Fig. 1a-b). The mean local time (MLT) equator crossing time of Terra gradually changed from 10:45 in the first two years until it reached its designed time around 10:30 (Davies et al., 2017). Terra made its final inclination adjustment maneuver to maintain its nominal orbit by the flight operations teams on 2020-02-27, after nearly 20 years of continuous earth observation (NSIDC, 2021). Terra will continue to drift, resulting in earlier overpass times. Similarly, Aqua's orbit began to drift to a later MLT from 2021-03-18, again leading to later overpass times. Orbital drift influences the local acquisition time (Fig. 1a-b), which induces variations in shadows (NSIDC, 2021), surface melt, viewing conditions, and the solar zenith and viewing zenith and azimuth angles. The viewing angles impact albedo estimates because the surface reflectance varies as a function of these two angles as described by the BRDF (Zhang and Roy, 2016; Ji and Brown, 2017) but since the angles are known to a high precision, this is accurately accounted for in MODIS albedo products using a BRDF correction, unless SZAs exceeding 75° (Stroeve et al., 2005, 2006; Schaaf et al., 2011a). Temporal consistency of cloud discrimination is another source of albedo error. For example, Davies et al. (2017) found a high frequency of cloud artifacts in the first two years (2000-2001) of records derived from the Multiangle Imaging Spectroradiometer (MISR) aboard Terra. We note that the image footprint also changes as the orbital drift progresses, with lower orbits resulting in smaller footprints. The MODIS albedo products utilized in this study are high level products that have been reprocessed to a coarser resolution than the lower level products. This minimizes the orbital drift effect on the effective spatial resolution, and so it was not analyzed further here.

In this study, we attempt to quantify the effect of orbital drift on time series of Terra MODIS snow albedo by comparison with 1) Aqua MODIS albedo, 2) a harmonized Landsat and Sentinel 2 derived albedo product (Feng et al., 2023), 3) a Sentinel 3 albedo product (Kokhanovsky et al., 2020, 2022; Wehrlé et al., 2021) and 4) Programme for Monitoring of the Greenland Ice Sheet (PROMICE) surface automatic weather stations (AWSs) (Van As and Fausto, 2011; Fausto et al., 2021).

2. Methods

2.1. Data processing

The Greenland ice sheet has a relatively flat, homogeneous surface away from the ice margin and is less cloudy than other Arctic regions, making it attractive for evaluating albedo products derived from satellite imagery (Stroeve et al., 2006). There is an extensive network of weather stations (Fig. 1c) for ground truthing. Our area of interest (AOI) is the entire ice sheet, defined by the ice mask from the Greenland Ice Mapping Project (Howat et al., 2014). In total, 17,793 sampling points were randomly generated with a 5 km buffer (Fig. 1c and d) in Google Earth Engine (GEE) (Gorelick et al., 2016), which is ten times coarser than the spatial resolution of the MODIS albedo data. This is to avoid the influence of spatial autocorrelation in the sampling sites (Olofsson et al., 2014; Ploton et al., 2020; Gorelick, 2021).

In total, four different albedo products (Table .1) were imported and processed. The MODIS albedo collection 006 includes considerable improvements, as suggested by validation with *in situ* observations (Wright et al., 2014; Hall et al., 2018), and was utilized in this study. The latest

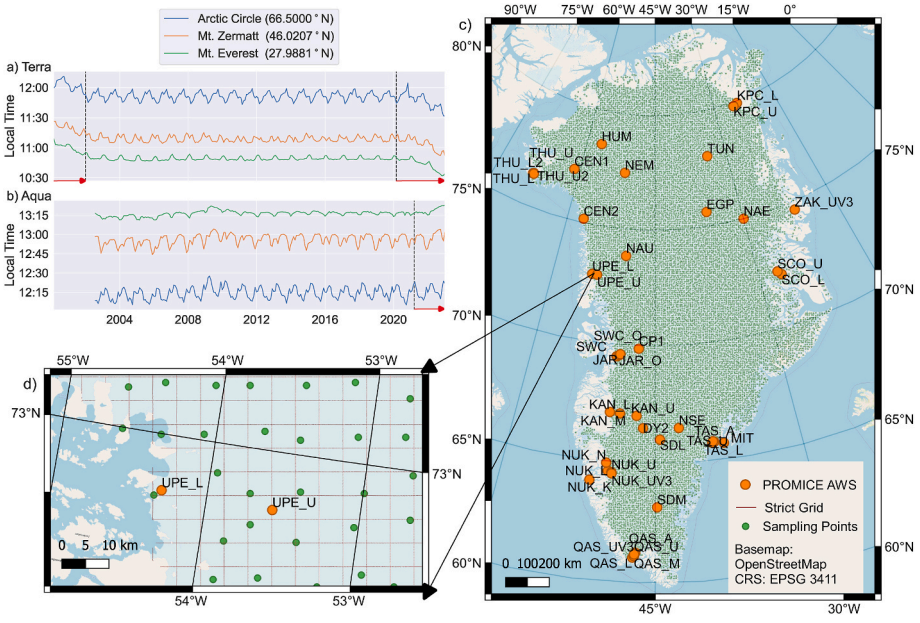

Fig. 1. The monthly average local image acquisition times of Terra (a) and Aqua (b) at different latitudes. The black dashed lines indicate periods of stable orbit: a) 2002-01-01 to 2020-02-27; b) 2002-07-04 to 2021-03-18. The Greenland ice sheet study area (c), and the random sampling points which were generated with a 5 km grid are shown by green dots (subfigure d). Locations of PROMICE/GC-Net AWSs (How et al., 2022) are marked as orange dots.

Table 1
Summary table of the spatial resolution and spectral band wavelengths of the utilized albedo products.

Data	Spatial Resolution (m)		Spectral Wavelength (nm)
	Original	Resampled	
MOD10	500	-	400-1400
MYD10	500	-	400-1400
HSA	30	500	400-865
S3 albedo	1000	500	400-1020

collection 6.1 was not yet fully ingested into GEE due to projection issues; therefore, collection 6 was utilized instead. The processing pipeline developed in GEE can be converted to collection 6.1 or 7 data once it is available in GEE. Hereafter, Terra MODIS albedo (MOD10A1.006) is referred to as MOD10 (Hall et al., 2016b) and Aqua MODIS albedo (MYD10A1.006) as MYD10 (Hall et al., 2016a). Snow and ice albedo is part of the Snow Albedo Daily Tile band. Invalid pixels are masked (Huang et al., 2022). A harmonized satellite albedo (HSA) dataset calculated from harmonized Landsat 4-9 and Sentinel 2 surface reflectance datasets (Feng et al., 2023) is used for comparative purposes using a 30 m ground resolution. Cloud and cloud shadows detected by Fmask (Zhu and Woodcock, 2012; Zhu et al., 2015) and Sen2Cor (Main-Knorn et al., 2017), gaps caused by the scan line error on Landsat 7, and saturated pixels were all masked. A daily Sentinel 3 ice albedo (S3 albedo) product with 1 km resolution has been produced by the ESA SICE project (http://snow.geus.dk/) (Kokhanovsky et al., 2020, 2022; Wehrlé et al., 2021). Invalid albedo values (< 0 or > 1) from all datasets were excluded from the analysis. The accuracy of MODIS albedo decreases at high SZAs, especially when SZA>75° (Stroeve et al., 2005, 2006; Schaaf et al., 2011a), so the study period was restricted to June through August (JJA), when SZA is minimal (Box et al., 2012), in order to avoid problematic albedo data. The albedo products used here span JJA of 2000-2022. The effect of orbital drift was assessed by the albedo data extracted from the randomly generated sampling points at 500 m scale.

Cloudiness influences the data density (Zhang et al., 2021), and information about the product quality influences the reliability of MODIS datasets (Schaaf et al., 2011a). Invalid MODIS albedo values consist of pixels classified by ten categories, namely, cloud, cloud detected as snow, ocean, land, night, self-shadowing, missing, inland water, non-production mask, BRDF failure, and no decision (Huang et al., 2022). Product quality data in the Snow Albedo Daily Tile Class band were extracted for the sampling sites to assess the effect of orbital drift on the availability of clear sky observations. The ground truth hourly cloud cover fraction is estimated from the downward longwave irradiance and near-surface air temperature (Van As et al., 2005; Fausto et al., 2021) by the PROMICE AWS network (Van As and Fausto, 2011; Fausto et al., 2021; How et al., 2022). PROMICE AWS Edition 4 dataset began in mid-2020 and includes a new generation of Greenland Climate Network (GC-Net) AWS (Steffen et al., 1996; Steffen and Box, 2001) carried forward by the Geological Survey of Denmark and Greenland (GEUS). The timestamps of AWS data were converted from Coordinated Universal Time (UTC) to local solar time.

2.2. Evaluation of orbital drift effect

The Terra MODIS albedo performs slightly better than the Aqua MODIS albedo when compared with *in situ* ground truth data (Stroeve et al., 2006) and is used more frequently in trend analysis because of its longer temporal coverage. The band 6 failure on Aqua MODIS has been restored by applying a Quantitative Image Restoration (QIR) (Gladkova et al., 2012; NSIDC, 2016). Aqua MODIS is a nearly identical copy of Terra MODIS (Barnes et al., 2003) and was not influenced by orbital drift until approximately one year after Terra, making it useful to evaluate the orbital drift effect of Terra MODIS. The HSA and S3 albedo were used to show the relative impact of orbital drift that is not covered by the nominal operational time of Aqua. The orbital drift effect was also evaluated at point scale using PROMICE *in situ* measurements.

The orbital drift effect, $d(t)$, was quantified by using Eqs. (1)–(3), adapted from Qiu et al. (2021), where i is the ith sampling point and $n = 17{,}793$ (Fig. 1c-d). All the extracted MOD10 point values were matched with MYD10, HSA, and S3 albedo using the timestamp ($dt \leq 1$ day) and the coordinates, so pairing the MOD10 albedo (α^{MOD10}) at each sampling point with the other reference albedo (α^{Ref}) data acquired on the same day. Paired pixel values with differences ($|\alpha_i^{MOD10} - \alpha_i^{Ref}|$) greater than their average value ($0.5|\alpha_i^{MOD10} + \alpha_i^{Ref}|$) were masked out from the analysis using a noise filter (Eq. (4)) adapted from Roy et al. (2016). The MOD10 data acquired in a nominal orbit (t_0 = 2002-2019) were compared with the reference albedo data to establish the baseline ($median\Delta\alpha(t_0)$) of albedo differences (Eq. (3)). Next, the MOD10 data within the drift period were compared with the paired α^{Ref}. The $d(t)$ was also quantified at pixel level for the entire ice sheet.

$$d(t) = median\Delta\alpha(t) - median\Delta\alpha(t_0) \tag{1}$$

$$median\Delta\alpha(t) = median\{\Delta\alpha_1(t), \Delta\alpha_2(t), \Delta\alpha_3(t), \ldots \Delta\alpha_n(t)\} \tag{2}$$

$$\Delta\alpha_i(t) = \alpha_i^{MOD10}(t) - \alpha_i^{Ref}(t) \tag{3}$$

$$\frac{|\alpha_i^{MOD10} - \alpha_i^{Ref}|}{0.5|\alpha_i^{MOD10} + \alpha_i^{Ref}|} < 1 \tag{4}$$

The cross sensor difference between MOD10 and MYD10 in 2002-2019 was measured by Eq. (3), and Eq. (2) calculated the $median\Delta\alpha_i(2002 - 2019)$ to establish the baseline of the cross sensor albedo difference. The median cross sensor difference ($median\Delta\alpha_i(2020)$) between MOD10 and MYD10 after Terra began to drift in 2020 was also derived. Finally, the orbital drift effect ($d(2020)$) was calculated by Eq. (1), which compares the cross sensor difference to the baseline value. Similarly, the HSA and S3 albedo were each used as the reference albedo to quantify the effect of orbital drift when MYD10 was unavailable (t = 2000-2001) or when Aqua also began to drift (t = 2021-2022). The orbits of Landsat 5 (2003-2007) and 7 (2017-present) were not as stable as Landsat 8 and may introduce temporal inconsistency to the surface reflectance data (Zhang and Roy, 2016; Roy et al., 2020; Qiu et al., 2021). Hence, the $d(2000 - 2001)$ was evaluated by the HSA ($t_0 = 2002$) and the $d(2020 - 2022)$ was evaluated by the HSA (t_0 = 2019, excluding Landsat 7) and the S3 albedo ($t_0 = 2019$).

The utilized albedo products were also compared with *in situ* PROMICE daily albedo data to test if the orbital drift effect can be quantified at point scale. MOD10, MYD10, HSA, and S3 albedo were extracted at the coordinates of the AWS UPE_L (Fig. 1d) and linearly correlated with the ground truth albedo to demonstrate the change in absolute error over time.

2.3. Processing tools and GEE web application

A GEE web application (MODIS-Orbit-Drift-Viewer, https://fsn1995.users.earthengine.app/view/modis-orbit-drift-viewer) is made to enable readers to visually inspect the orbital drift effect (d(t)) and extract summer (JJA) time series data of d(t), MOD10, and MYD10 at any point of interest. The d(t) map covers the entire ice sheet and ice covered areas using the ice mask from the Greenland Ice Mapping Project (Howat et al., 2014) and the Global Land Ice Measurements From Space (GLIMS) Current database (GLIMS Consortium, 2005; Raup et al., 2007). The assessment of future MODIS albedo products will be updated in the web app once new versions become available on GEE. All the scripts for processing and analysis are available on GitHub https://github.com/fsn1995/orbit-drift-MODIS-ice-albedo and Zenodo (Feng, 2023). https://doi.org/10.22008/FK2/IW73UU. The MODIS albedo, Landsat, and Sentinel 2 data are available on GEE and are processed mainly using GEE's code editor, geemap (Wu, 2020; Wu et al., 2019) and

the Arctic Mapping Tools (Greene et al., 2017). The colormap is from the cmocean package (Thyng et al., 2016).

3. Results

3.1. Cloudiness and data density

The temporal resolution of MOD10 is daily, but the effective temporal resolution (frequency of clear observations) is influenced by cloud cover and various other relatively minor factors (Fig. 2a). Cloud data comprises more than 93% of all the invalid pixel values in the entire study period, except 2000 (Fig. 2a). The number of invalid pixels increased as the image acquisition time progressively became earlier after the orbital drift started in 2020 (Fig. 2a), in contrast with the trend of annual cloud cover in the *in situ* records. The median 2022 cloud cover from PROMICE/GC-Net AWSs (Fig. 2b) was significantly lower than in 2021 according to a left-tailed Wilcoxon rank sum test ($p < 0.01$). Yet, the number of cloud pixels in 2022 was 66% more than in 2021, and was triple the average in the pre-orbital drift period (2002 to 2019), suggesting that systematic changes in acquisition time influenced the number of cloud contaminated pixels. The diurnal variations of AWS cloud cover are shown in Fig. 2c-d.

3.2. Orbital drift effect

The quantification of the orbital drift effect focused on evaluating the temporal consistency of the albedo values. Analysis was undertaken at regional scale (Fig. 3a-b), aggregated random sampling scale (Fig. 3c), and point scale (Fig. 5).

The reference MYD10 was used for the spatial evaluation of the orbital drift effect. The albedo difference between MOD10 and MYD10 ($median\Delta\alpha$(2002-2019), Eq. (2)) was negligible for most of the ice sheet ($median = 0$, $std = 0.017$) (Fig. 3a), although outliers occur in the northeast and northwest. The MOD10 and MYD10 values agreed well during the nominal operation ($median\Delta\alpha(2002 - 2019) = 0$). The orbital drift effect ($d(2020)$, Eq. (1)) was more spatially variable (Fig. 3b).

The overall $d(t)$ was consolidated for the sampling points and was evaluated using the reference MYD10, S3 albedo, and HSA. Generally, MOD10 became increasingly positively biased ($d(2020) = +0.01$, Fig. 3b-c) relative to MYD10, HSA, and S3 albedo as the MODIS orbital drift began in 2020. The trend of $d(t)$ estimated by S3 albedo was constant ($d(2021)$ and $d(2022) = +0.01$). The orbital drift of Terra occurred in the first two years of operation and cannot be assessed using MYD10 after 2020. The HSA estimated discrepancy with MOD10 in 2020 was double the MYD10 estimated drift effect, and the increasing trend of the orbital drift effect in 2020-2022 was systematic ($+0.02 \cdot a^{-1}$). The orbital drift effect in 2000-2001 was negative, indicating that MOD10 decreased relative to the HSA, but the estimated $d(2000 - 2001)$ values were less reliable as the orbit of Landsat 5 was not as stable as Landsat 8 (Qiu et al., 2021).

The estimated d(t) is relatively small, but it is important to understand its impact on time series of albedo. The long-term trend of albedo in the pre-drift period (2002-2019) is $-0.0004 \cdot a^{-1}$, but the albedo decline rate calculated for the period 2002-2020, after the orbital drift started, is $-0.0003 \cdot a^{-1}$ because of the increased average JJA albedo in 2020 (Fig. 4). He et al. (2013) found that the albedo decline was more significant around the year 2000. We excluded the period (2000-2001) from our analysis because Terra was in its designated orbit in these two years, and so orbital drift may have influenced albedo accuracy in this period too.

The orbital drift effect evaluated at point scale using *in situ* AWS daily albedo measurements (black line in Fig. 5) from AWS UPE_L is shown in Fig. 5. It is to test if the orbital drift effect can be quantified by AWS albedo observations. The agreements between the ground truth albedo and the satellite derived albedo products had Pearson's R values of 0.63 (slope = 0.42) for MOD10, 0.74 (slope = 0.60) for MYD10, 0.80 (slope = 0.69) for HSA, and 0.84 (slope = 0.64) for S3 with $p < 0.05$ (Fig. 5e-h). The correlation of MOD10 deteriorated over time (R decreased from 0.79 in 2020 to 0.50 in 2021, and 0.40 in 2022, $p < 0.05$, and the Root Mean Squared Error increased from 0.07 to 0.10 from 2020 to 2022). The deterioration in correlation is only obvious in the UPE_L data compared to other PROMICE AWSs in the Dark Zone and EGP, which is a site in a perennially snow-covered area in northeast Greenland. Thus, ground measurements may not be suitable for quantifying the orbital drift effect, as the correlation between MOD10 and *in situ* AWS albedo can be influenced by various factors (e.g., the difference in spatial resolution, AWS condition, and seasonal variations in ice surface homogeneity).

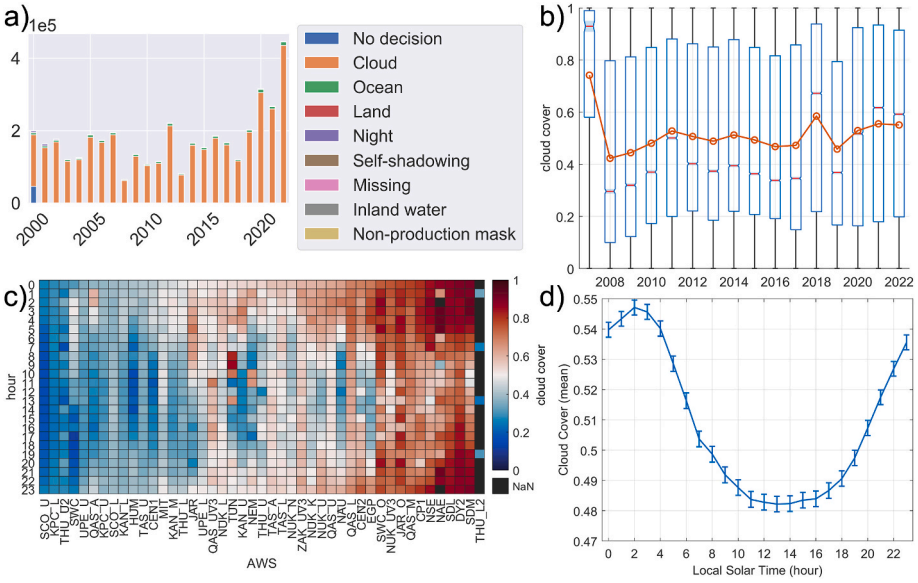

Fig. 2. a) Annual invalid MOD10 variations June through August (JJA) from 2000 to 2022 by class, revealing the dominant effect of clouds. Notched boxplot (b) of annual variations in JJA automatic weather station (AWS) cloud cover index 2007-2022 with the average value as the red line. (c) median hourly cloud cover for data from individual AWS used here. (d) hourly average AWS cloud cover includes standard error whiskers.

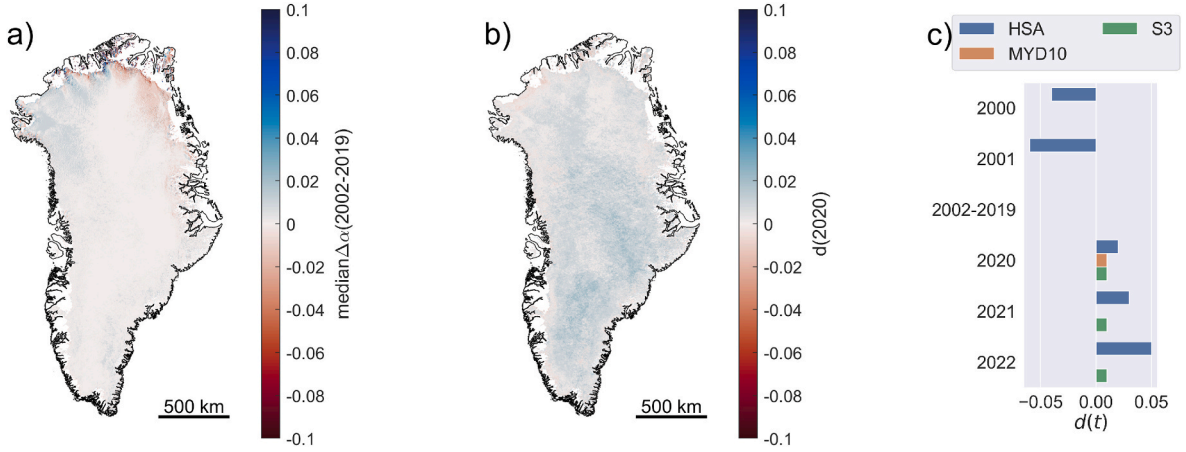

Fig. 3. Quantification of the orbital drift effect on MOD10. Maps of pixel-wise *median*$\Delta\alpha$(2002-2019) and d(2020) calculated using MYD10 are illustrated in subfigures a and b, respectively. The drift effect ($d(t)$, subfigure c) derived from the sampling points is calculated using the HSA, MYD10, and S3 albedo.

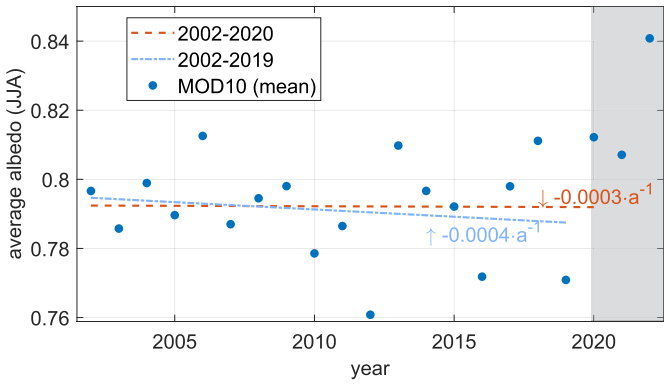

Fig. 4. Time series of average JJA albedo and the long-term trend for the period 2002-2019 and the period 2002-2020. The albedo is the sampled MOD10 albedo data and the grey-shaded area shows the data influenced by the orbital drift of Terra.

4. Discussion

4.1. Cloudiness and data density

Orbital drift directly influences the image acquisition time of MOD10 (NSIDC, 2021). The mean local time (MLT) varies latitudinally (Levy et al., 2018), and gradually changed by 14 min at the Arctic Circle from 12:06 (2000) to about 11:52 (2002-2019). Terra progressively drifted to give an MLT that was 27 min earlier (11:39) in 2022 (Fig. 1a). A threefold increase in MOD10 cloud pixels occurred after the orbital drift began in 2020, yet an increase in cloud frequency is not observed in the AWS data (Fig. 2b). However, we do not yet have sufficient data to test whether this is a source of error in the albedo product. We note that we did not observe an increase in cloud frequency in the AWS data, but on the other hand, the AWS data is coarse and limited in spatial coverage.

Generally, summer clouds in the Arctic form in the morning, dissipate near the solar noon and accumulate again in the afternoon (Shupe et al., 2011). The cloud cover fraction across the ice sheet varies depending on the hour of the day (Fig. 2d) and the location (Fig. 2c). The number of clear observations is influenced by the satellite overpassing time (King et al., 2013; Tang et al., 2020). The trend towards earlier satellite overpassing times could, in principle, account for some of the increase in invalid MOD10 pixels predominated by clouds (Fig. 2a), but we find that an increase in cloud pixels is not evident in *in situ* AWS cloud index data. Both Terra MODIS and Aqua MODIS are to remain operational until 2025 and 2026, respectively (NSIDC, 2021), and it may well be that earlier image acquisition times lead to more apparent cloud cover in MODIS imagery, so impacting the availability and utility of images (Fig. 2a). The temporal resolution of bare ice albedo is crucial for the performance of regional melt models (Irvine-Fynn et al., 2021), and so less dense observations may handicap time series analysis (Qiu et al., 2021) using MOD10.

We examined the statistical significance of the apparent decrease in cloud cover measured by the AWS from 11:00 to 12:00 by a right-tailed Wilcoxon signed rank test, which indicated a weak relationship ($p = 0.07$). We note that cloud frequency is highly variable and it is possible that the point scale PROMICE AWS measurements may not capture the spatial and temporal variations of clouds over the ice sheet in the same way as from the relatively much wider coverage that is obtained from satellite swath data. Hence, we can only highlight the discrepancy between the two data sets, that satellite imagery shows increasing cloud cover whereas AWS measurements do not, and can provide no clear explanation for the discrepancy at present. The change in cloudiness being a mechanism for the observed effects of orbital drift remains a hypothesis that can be more rigorously tested with additional data (e.g., cloud cover fraction data derived from geostationary satellites like the Geostationary Operational Environmental Satellite (GOES) (Schmit et al., 2017; Bah et al., 2018) and/or climate reanalysis dataset like the Modern-Era Retrospective Analysis for Research and Applications (MERRA) (Rienecker et al., 2011)) in the future, and as the orbital drift increases, the overpass time change.

4.2. Absolute albedo consistency

The orbital drift of Terra has a limited but measurable impact on the absolute accuracy and consistency of MOD10 albedo. The MYD10 estimated orbital drift effect is small ($d(2020) = +0.01$), but may be critical because the long term trend in albedo reduction over the ice sheet is relatively small ($[-0.0060, -0.0028] \cdot a^{-1}$) (Box et al., 2012; He et al., 2013; Alexander et al., 2014) and appears insignificant. The positive bias of albedo may become increasingly important after including the recent years (2015-2020) when the albedo decline rate is further reduced (Fig. 4). The reliability of trend detection will deteriorate over time if the MOD10 generally becomes increasingly positively biased relative to the reference albedo (Fig. 3c). The orbital drift effect also varies spatially (Fig. 3b) and so is not homogeneous. Therefore, any orbital drift correction factor may need to account for pixel-by-pixel variability. Trend analysis using MOD10 influenced by the orbital drift needs to be conducted with caution.

Comparison and evaluation of alternative products are necessary to ensure the continuity of observation records (Riggs and Hall, 2020) as the orbital drift progresses or when MODIS reaches the end of its

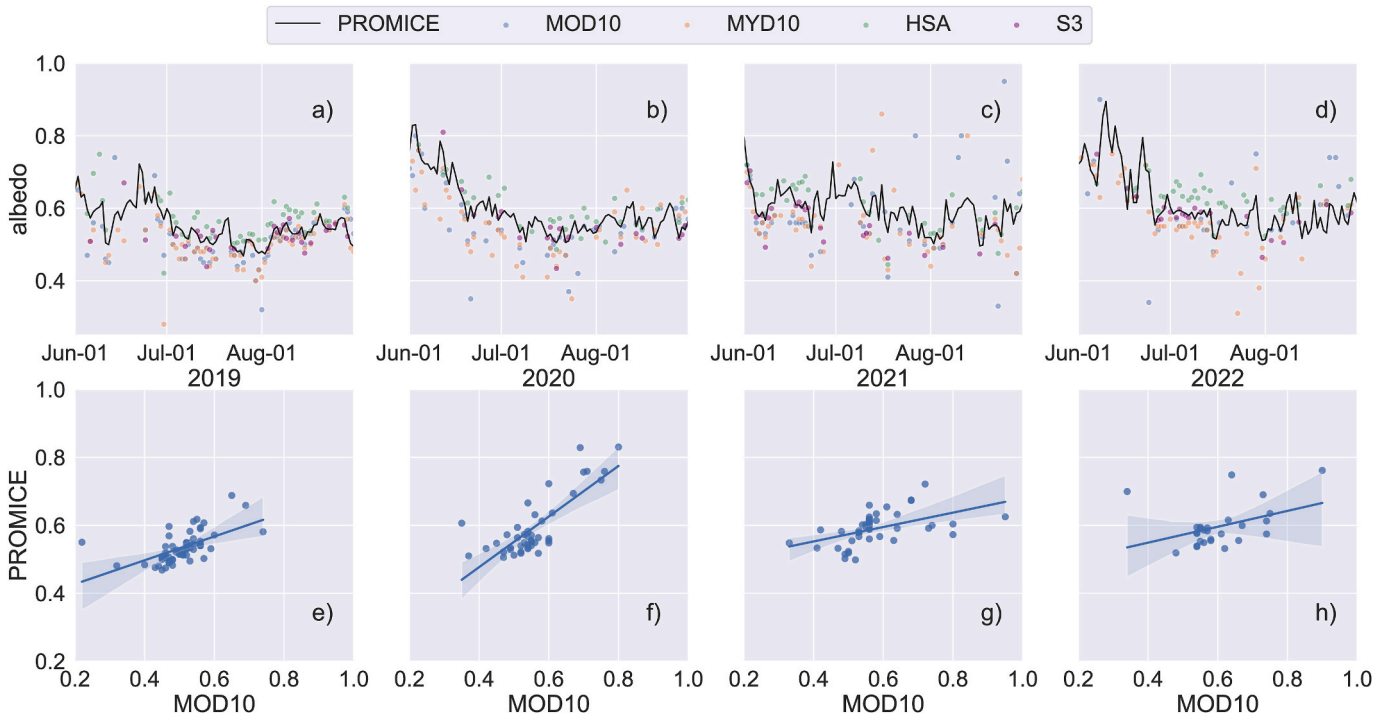

Fig. 5. Time series of albedo at PROMICE AWS UPE_L (location is shown in Fig. 1c-d) during summer (June through August) 2019-2022 (a-d). Albedo data include PROMICE AWS daily measurements, MOD10, MYD10, HSA, and S3 albedo. Lower panel (e-h) shows the scatterplots and the linear regressions between MOD10 and PROMICE AWS albedo.

lifetime. HSA has a higher spatial resolution (30 m), and S3 albedo is reprocessed to a daily product comparable to MOD10. Both the HSA and the S3 albedo are good alternatives and correlate well with *in situ* AWS albedo (Fig. 5).

4.3. Uncertainties

Uncertainties in cross sensor comparison of ice albedo products can result from cloud contamination, differences in effective spatial resolution, and other factors, such as image acquisition time, viewing geometry, and surface melt (Liu et al., 2017; Riggs and Hall, 2020). The orbital drift effect estimated by using the MYD10 is the most reliable, as the similarities between MOD10 and MYD10 help minimize the uncertainties. The orbital drift effect estimated using an independent reference albedo data set, such as the HSA and S3 albedo, is indicative, due to the cross sensor differences. However, the cross sensor comparison could help us estimate the trend of the orbital drift effect after MYD10 began to drift.

The MCD43A3, hereafter referred to as MCD43, albedo product provides both directional hemispherical reflectance (black sky albedo) and bihemispherical reflectance (white sky albedo) (Schaaf et al., 2002, 2011b), and has also been well validated and calibrated (Stroeve et al., 2005, 2013). The reason we chose MOD10 over MCD43 products is because of the wide MOD10 data user-base, including a) the Bulletin of the AMS (BAMS) State of the Climate reporting, the orbital issue relevant for the most recent two BAMS reports (Blunden and Boyer, 2022; Blunden et al., 2023), and b) the Copernicus Arctic Regional Re-analysis dataset (Køltzow et al., 2022). MOD10 is a popular product that has been widely used in studies that focus on the darkening of the Greenland Ice Sheet and the Dark Zone, for example, Box et al. (2012, 2022), Ryan et al. (2017, 2019), Tedstone et al. (2017, 2020), Wang et al. (2020), and Williamson et al. (2020). We note that Box et al. (2017) conducted a more comprehensive validation of MOD10 data than that of an earlier MCD43 data validation (Stroeve et al., 2013). These validation results suggest that both are well calibrated and are reliable albedo products, but Casey et al. (2017) found that trend analysis using the MCD43 C6 dataset can lead to false statistically significant trends due to a calibration error. Terra MODIS and Aqua MODIS are near identical sensors, and orbital drift did not occur to Aqua until about a year after Terra. Therefore, the impact of orbital drift should be different because Terra and Aqua began to drift at different times, and Terra is drifting towards earlier acquisition time while Aqua is drifting towards later acquisition time. It is important to treat the sensors separately. Eq. (1)) quantifies the orbital drift effect by calculating the deviations of albedo influenced by orbital drift relative to the reference albedo. However, the MCD43 product was generated by using both MODIS Terra and MODIS Aqua. The orbital drift effect of two sensors is mixed in MCD43, and it is challenging to separate MODIS Terra and MODIS Aqua data in MCD43. Therefore, the orbital drift effect on the MCD43 albedo was not analyzed. The calibration drift error was not considered in this study because it has not been found in the MOD10 dataset (Casey et al., 2017). Major updates on the MODIS sensor calibration will be made by NASA to mitigate the degradation and keep the data consistency of future Collection 7 (C7) MODIS products (Angal et al., 2023; Xiong et al., 2023). We plan to re-evaluate the orbital drift effect of both MOD10 and MCD43 when the better calibrated C7 datasets are available.

MODIS albedo is positively biased relative to *in situ* measurements over the ablation area (Stroeve et al., 2013; Ryan et al., 2017) mostly because coarser resolution albedo data have more limited capability of detecting local scale albedo changes, which are often on finer spatial scales (Tedstone et al., 2020). The HSA was resampled from 30 m to 500 m, but it cannot fully address the differences introduced by the spatial resolution. The image resolution of S3 is 300 m, and the S3 albedo product is resampled to 1 km, which is more similar to MOD10 than HSA. Further, the spatial resolution of MODIS pixels is about 20 times larger than the footprint of the AWS albedo data, so confounding easy comparison of the data sets. Therefore, it is hard to discriminate the effect of orbital drift from noises introduced by the mismatch between the ground sampling distance of AWS at point scale and satellite sensors with coarser resolutions (Fig. 5). In our future studies, we aim to use

both the reprocessed historical GC-Net AWS dataset and PROMICE AWS dataset to reevaluate the orbital drift effect, sensor degradation, and sensor calibration issues associated with MODIS data. The uncertainties in the orbital drift effect estimated by the HSA are inherently greater. The reference HSA is also not free from the impact of orbital drift, but the influence should be small as the time of interest did not include the years (1995 for Landsat 5 and after 2020 for Landsat 7) when the impact of orbital drift was most significant (Zhang and Roy, 2016; Roy et al., 2020; Qiu et al., 2021).

5. Conclusion

The orbital drift of the NASA Terra satellite has led to a progressively earlier image acquisition time since 2020 by over 24 min at the Arctic Circle. The comparison with reference albedo products in nominal orbits incurred a small impact ($d(2020) = +0.01$) on the temporal consistency, and the bias is expected to increase in the future. The positive bias relative to the reference albedo products is small, but it may be substantial for trend analysis when the real trend is smaller than the artifact induced by the orbital drift. The impact of orbital drift-related bias on other glaciological applications that do not require high accuracy in the absolute albedo values (e.g., snowline migration monitoring, mass balance modeling, snow-free durations) should still be negligible. In summer, a diurnal cloud development cycle, in combination with the orbit drift causing an earlier satellite overpass time, may give rise to more pixels affected by clouds, decreasing the number of clear observations. The influence on the data density in time series analysis, varying due to the overpass time drift interaction with diurnal cloud development, should also be taken into consideration in future studies. It is possible that MODIS products may confirm this trend or other puzzles to solve, but this will involve an analysis of the channels utilized and the algorithms used to produce the products under consideration. A more comprehensive evaluation of MODIS orbital drift effects on data consistency, the effective image footprint, the BRDF effect, future orbital drift trends, and the continuity of MODIS products using alternative sensors should be conducted in the future. The analysis presented in this paper will be useful for future studies that aim to generate orbital-drift corrected albedo products.

CRediT authorship contribution statement

Shunan Feng: Writing – review & editing, Writing – original draft, Visualization, Validation, Software, Resources, Methodology, Investigation, Formal analysis, Data curation, Conceptualization. **Adrien Wehrlé:** Writing – review & editing, Software, Data curation. **Joseph Mitchell Cook:** Writing – review & editing, Supervision, Project administration. **Alexandre Magno Anesio:** Writing – review & editing, Supervision, Funding acquisition, Project administration. **Jason Eric Box:** Writing – review & editing, Validation, Investigation. **Liane G. Benning:** Writing – review & editing, Project administration, Funding acquisition. **Martyn Tranter:** Writing – review & editing, Supervision, Project administration, Funding acquisition.

Declaration of competing interest

The authors declare that they have no known competing financial interests or personal relationships that could have appeared to influence the work reported in this paper.

Data availability

All the utilized data are available on Google Earth Engine and GEUS Dataverse. The Sentinel 3 albedo will be available shortly on GEUS Dataverse. The scripts are available on GitHub.

Acknowledgments

This publication is part of the Deep Purple Project. The project receives funding from the European Research Council (ERC) under the European Union's Horizon 2020 research and innovation program under grant agreement No. 856416.

We would like to express our gratitude to the PROMICE team and thank Penelope How for her help with PROMICE data. We are very grateful for the insightful commentary and suggestions from three anonymous reviewers, which greatly improved the quality of this manuscript and provided valuable guidance for future work. Furthermore, we wish to express great thanks to the editors, Peter Michael Atkinson and Joseph Awange, for their dedicated support throughout the review process.

References

Alexander, P.M., Tedesco, M., Fettweis, X., van de Wal, R.S.W., Smeets, C.J.P.P., van den Broeke, M.R., 2014. Assessing spatio-temporal variability and trends in modelled and measured Greenland Ice Sheet albedo (2000–2013). Cryosphere 8, 2293–2312. https://doi.org/10.5194/tc-8-2293-2014.

Angal, A., Xiong, X., Twedt, K., Chang, T., Geng, X., Aldoretta, E., Díaz, C.P., 2023. Status of the terra and aqua MODIS collection 7 L1B. In: IEEE IGARSS Conference, pp. 4466–4469. Pasadena.

Bah, M.K., Gunshor, M.M., Schmit, T.J., 2018. Generation of GOES-16 true color imagery without a green band. Earth Space Sci. 5, 549–558. URL. https://agupubs.onlinelibrary.wiley.com/doi/10.1029/2018EA000379, 10.1029/2018EA000379.

Barnes, W., Xiong, X., Salomonson, V., 2003. Status of terra MODIS and aqua modis. Adv. Space Res. 32, 2099–2106. https://doi.org/10.1016/S0273-1177(03)90529-1.

Blunden, J., Boyer, T., 2022. State of the climate in 2021. Bull. Am. Meteorol. Soc. 103, S1–S465. https://doi.org/10.1175/2022BAMSStateoftheClimate.1.

Blunden, J., Boyer, T., Bartow-Gillies, E., 2023. State of the climate in 2022. Bull. Am. Meteorol. Soc. 104, S1–S516. https://doi.org/10.1175/2023BAMSStateoftheClimate.1.

Box, J.E., Fettweis, X., Stroeve, J.C., Tedesco, M., Hall, D.K., Steffen, K., 2012. Greenland ice sheet albedo feedback: thermodynamics and atmospheric drivers. Cryosphere 6, 821–839. https://doi.org/10.5194/tc-6-821-2012.

Box, J.E., As, D.v., Steffen, K., 2017. Greenland, Canadian and Icelandic land-ice albedo grids (2000–2016). GEUS Bulletin 38, 53–56. https://doi.org/10.34194/GEUSB.V38.4414.

Box, J.E., Hubbard, A., Bahr, D.B., Colgan, W.T., Fettweis, X., Mankoff, K.D., Wehrlé, A., Noël, B., van den Broeke, M.R., Wouters, B., Bjørk, A.A., Fausto, R.S., 2022. Greenland ice sheet climate disequilibrium and committed sea-level rise. Nat. Clim. Change 1–6. https://doi.org/10.1038/s41558-022-01441-2.

Casey, K.A., Polashenski, C.M., Chen, J., Tedesco, M., 2017. Impact of MODIS sensor calibration updates on Greenland Ice Sheet surface reflectance and albedo trends. Cryosphere 11, 1781–1795. https://doi.org/10.5194/tc-11-1781-2017.

Cook, J.M., Hodson, A.J., Gardner, A.S., Flanner, M., Tedstone, A.J., Williamson, C., Irvine-Fynn, T.D.L., Nilsson, J., Bryant, R., Tranter, M., 2017. Quantifying bioalbedo: a new physically based model and discussion of empirical methods for characterising biological influence on ice and snow albedo. Cryosphere 11, 2611–2632. https://doi.org/10.5194/tc-11-2611-2017.

Cook, J.M., Tedstone, A.J., Williamson, C., McCutcheon, J., Hodson, A.J., Dayal, A., Skiles, M., Hofer, S., Bryant, R., McAree, O., McGonigle, A., Ryan, J., Anesio, A.M., Irvine-Fynn, T.D.L., Hubbard, A., Hanna, E., Flanner, M., Mayanna, S., Benning, L.G., van As, D., Yallop, M., McQuaid, J.B., Gribbin, T., Tranter, M., 2020. Glacier algae accelerate melt rates on the south-western Greenland Ice Sheet. Cryosphere 14, 309–330. https://doi.org/10.5194/tc-14-309-2020.

Davies, R., Jovanovic, V.M., Moroney, C.M., 2017. Cloud heights measured by MISR from 2000 to 2015. J. Geophys. Res. Atmos. 122, 3975–3986. https://doi.org/10.1002/2017JD026456.

Dietz, A.J., Kuenzer, C., Dech, S., 2015. Global SnowPack: a new set of snow cover parameters for studying status and dynamics of the planetary snow cover extent. Remote Sensing Letters 6, 844–853. https://doi.org/10.1080/2150704X.2015.1084551.

Fausto, R.S., van As, D., Mankoff, K.D., Vandecrux, B., Citterio, M., Ahlstrøm, A.P., Andersen, S.B., Colgan, W., Karlsson, N.B., Kjeldsen, K.K., Korsgaard, N.J., Larsen, S. H., Nielsen, S., Pedersen, A.Ø., Shields, C.L., Solgaard, A.M., Box, J.E., 2021. Programme for Monitoring of the Greenland Ice Sheet (PROMICE) automatic weather station data. Earth Syst. Sci. Data 13, 3819–3845. https://doi.org/10.5194/essd-13-3819-2021.

Feng, S., 2023. fsn1995/orbit-drift-MODIS-ice-albedo: Orbital Drift Effect of MODIS Ice Albedo. https://doi.org/10.5281/zenodo.8040445.

Feng, S., Cook, J.M., Anesio, A.M., Benning, L.G., Tranter, M., 2023. Long time series (1984–2020) of albedo variations on the Greenland ice sheet from harmonized Landsat and Sentinel 2 imagery. J. Glaciol. 1–16. https://doi.org/10.1017/jog.2023.11.

Giglio, L., Roy, D.P., 2022. Assessment of satellite orbit-drift artifacts in the long-term AVHRR FireCCILT11 global burned area data set. Science of Remote Sensing 5, 100044. https://doi.org/10.1016/j.srs.2022.100044.

Gladkova, I., Grossberg, M.D., Shahriar, F., Bonev, G., Romanov, P., 2012. Quantitative restoration for MODIS band 6 on aqua. IEEE Trans. Geosci. Rem. Sens. 50, 2409–2416. https://doi.org/10.1109/TGRS.2011.2173499.
GLIMS Consortium, 2005. GLIMS Glacier Database, Version 1.
Gorelick, N., 2021. Random Samples with Buffering. Earth Engine by Example. URL. https://medium.com/google-earth/random-samples-with-buffering-6c8737384f8c.
Gorelick, N., Hancher, M., Dixon, M., Ilyushchenko, S., Thau, D., Moore, R., 2016. Google earth engine: planetary-scale geospatial analysis for everyone. Rem. Sens. Environ. 202, 18–27. https://doi.org/10.1016/j.rse.2017.06.031.
Greene, C.A., Gwyther, D.E., Blankenship, D.D., 2017. Antarctic mapping Tools for matlab. Comput. Geosci. 104, 151–157. https://doi.org/10.1016/j.cageo.2016.08.003.
Hall, D.K., Riggs, G.A., 2007. Accuracy assessment of the MODIS snow products. Hydrol. Process. 21, 1534–1547. https://doi.org/10.1002/hyp.6715.
Hall, D.K., Riggs, G.A., Salomonson, V.V., 1995. Development of methods for mapping global snow cover using moderate resolution imaging spectroradiometer data. Rem. Sens. Environ. 54, 127–140. https://doi.org/10.1016/0034-4257(95)00137-P.
Hall, D.K., Salomonson, V.V., Riggs, G.A., 2016a. MODIS/Aqua Snow Cover Daily L3 Global 500m Grid. https://doi.org/10.5067/MODIS/MYD10A1.006. Version 6.
Hall, D.K., Salomonson, V.V., Riggs, G.A., 2016b. MODIS/Terra Snow Cover Daily L3 Global 500m Grid. https://doi.org/10.5067/MODIS/MOD10A1.006. Version 6.
Hall, D.K., Cullather, R., DiGirolamo, N., Comiso, J., Medley, B., Nowicki, S., 2018. A multilayer surface temperature, surface albedo, and water vapor product of Greenland from MODIS. Rem. Sens. 10, 555. https://doi.org/10.3390/rs10040555.
He, T., Liang, S., Yu, Y., Wang, D., Gao, F., Liu, Q., 2013. Greenland surface albedo changes in July 1981–2012 from satellite observations. Environ. Res. Lett. 8, 044043 https://doi.org/10.1088/1748-9326/8/4/044043.
How, P., Mankoff, K.D., Wright, P.J., Vandecrux, B., Ahlstrøm, A.P., Fausto, R.S., 2022. AWS One Boom Tripod Edition, 4. https://doi.org/10.22008/FK2/IW73UU.
Howat, I.M., Negrete, A., Smith, B.E., 2014. The Greenland Ice Mapping Project (GIMP) land classification and surface elevation data sets. Cryosphere 8, 1509–1518. https://doi.org/10.5194/tc-8-1509-2014.
Huang, Y., Song, Z., Yang, H., Yu, B., Liu, H., Che, T., Chen, J., Wu, J., Shu, S., Peng, X., Zheng, Z., Xu, J., 2022. Snow cover detection in mid-latitude mountainous and polar regions using nighttime light data. Rem. Sens. Environ. 268, 112766 https://doi.org/10.1016/j.rse.2021.112766.
Irvine-Fynn, T.D.L., Bunting, P., Cook, J.M., Hubbard, A., Barrand, N.E., Hanna, E., Hardy, A.J., Hodson, A.J., Holt, T.O., Huss, M., McQuaid, J.B., Nilsson, J., Naegeli, K., Roberts, O., Ryan, J.C., Tedstone, A.J., Tranter, M., Williamson, C.J., 2021. Temporal variability of surface reflectance supersedes spatial resolution in defining Greenland's bare-ice albedo. Rem. Sens. 14, 62. https://doi.org/10.3390/rs14010062.
Ji, L., Brown, J.F., 2017. Effect of NOAA satellite orbital drift on AVHRR-derived phenological metrics. Int. J. Appl. Earth Obs. Geoinf. 62, 215–223. https://doi.org/10.1016/j.jag.2017.06.013.
Kaufmann, R., Zhou, L., Knyazikhin, Y., Shabanov, V., Myneni, R., Tucker, C., 2000. Effect of orbital drift and sensor changes on the time series of AVHRR vegetation index data. IEEE Trans. Geosci. Rem. Sens. 38, 2584–2597. https://doi.org/10.1109/36.885205.
King, M.D., Platnick, S., Menzel, W.P., Ackerman, S.A., Hubanks, P.A., 2013. Spatial and temporal distribution of clouds observed by MODIS onboard the terra and aqua satellites. IEEE Trans. Geosci. Rem. Sens. 51, 3826–3852. https://doi.org/10.1109/TGRS.2012.2227333.
Klein, A.G., Stroeve, J.C., 2002. Development and validation of a snow albedo algorithm for the MODIS instrument. Ann. Glaciol. 34, 45–52. https://doi.org/10.3189/172756402781817662.
Kokhanovsky, A., Box, J.E., Vandecrux, B., Mankoff, K.D., Lamare, M., Smirnov, A., Kern, M., 2020. The determination of snow albedo from satellite measurements using fast atmospheric correction technique. Rem. Sens. 12 https://doi.org/10.3390/rs12020234.
Kokhanovsky, A., Vandecrux, B., Wehrlé, A., Danne, O., Brockmann, C., Box, J.E., 2022. An improved retrieval of snow and ice properties using spaceborne OLCI/S-3 spectral reflectance measurements: updated atmospheric correction and snow impurity load estimation. Rem. Sens. 15, 77. https://doi.org/10.3390/rs15010077.
Køltzow, M., Schyberg, H., Støylen, E., Yang, X., 2022. Value of the Copernicus Arctic Regional Reanalysis (CARRA) in representing near-surface temperature and wind speed in the north-east European Arctic. Polar Res. 41, 8002. https://doi.org/10.33265/polar.v41.8002.
Levy, R.C., Mattoo, S., Sawyer, V., Shi, Y., Colarco, P.R., Lyapustin, A.I., Wang, Y., Remer, L.A., 2018. Exploring systematic offsets between aerosol products from the two MODIS sensors. Atmos. Meas. Tech. 11, 4073–4092. https://doi.org/10.5194/amt-11-4073-2018.
Liang, S., 2005. Mapping daily snow/ice shortwave broadband albedo from Moderate Resolution Imaging Spectroradiometer (MODIS): the improved direct retrieval algorithm and validation with Greenland in situ measurement. J. Geophys. Res. 110, D10109 https://doi.org/10.1029/2004JD005493.
Liu, Y., Wang, Z., Sun, Q., Erb, A.M., Li, Z., Schaaf, C.B., Zhang, X., Román, M.O., Scott, R.L., Zhang, Q., Novick, K.A., Syndonia Bret-Harte, M., Petroy, S., SanClements, M., 2017. Evaluation of the VIIRS BRDF, Albedo and NBAR products suite and an assessment of continuity with the long term MODIS record. Rem. Sens. Environ. 201, 256–274. https://doi.org/10.1016/j.rse.2017.09.020.
Macander, M.J., Swingley, C.S., Joly, K., Raynolds, M.K., 2015. Landsat-based snow persistence map for northwest Alaska. Rem. Sens. Environ. 163, 23–31. https://doi.org/10.1016/j.rse.2015.02.028.
Main-Knorn, M., Pflug, B., Louis, J., Debaecker, V., Müller-Wilm, U., Gascon, F., 2017. Sen2Cor for sentinel-2. In: Bruzzone, L., Bovolo, F., Benediktsson, J.A. (Eds.), Image and Signal Processing for Remote Sensing XXIII. SPIE, p. 3. https://doi.org/10.1117/12.2278218.
Naegeli, K., Damm, A., Huss, M., Wulf, H., Schaepman, M., Hoelzle, M., 2017. Cross-comparison of albedo products for glacier surfaces derived from airborne and satellite (Sentinel-2 and Landsat 8) optical data. Rem. Sens. 9, 110. https://doi.org/10.3390/rs9020110.
Naegeli, K., Huss, M., Hoelzle, M., 2019. Change detection of bare-ice albedo in the Swiss Alps. Cryosphere 13, 397–412. https://doi.org/10.5194/tc-13-397-2019.
Noël, B., van de Berg, W.J., Lhermitte, S., van den Broeke, M.R., 2019. Rapid ablation zone expansion amplifies north Greenland mass loss. Sci. Adv. 5 https://doi.org/10.1126/sciadv.aaw0123.
NSIDC, 2016. MODIS version history | national snow and ice data center. URL: https://nsidc.org/data/modis/version-history.
NSIDC, 2021. Ongoing changes in terra and aqua orbits impacting MODIS snow and sea ice products | national snow and ice data center. URL: https://nsidc.org/data/data-announcements/ongoing-changes-terra-and-aqua-orbits-impacting-modis-snow-and-sea-ice.
Olofsson, P., Foody, G.M., Herold, M., Stehman, S.V., Woodcock, C.E., Wulder, M.A., 2014. Good practices for estimating area and assessing accuracy of land change. Rem. Sens. Environ. 148, 42–57. https://doi.org/10.1016/J.RSE.2014.02.015.
Østby, T.I., Vikhamar Schuler, T., Ove Hagen, J., Hock, R., Kohler, J., Reijmer, C.H., 2017. Diagnosing the decline in climatic mass balance of glaciers in Svalbard over 1957-2014. Cryosphere 11, 191–215. https://doi.org/10.5194/tc-11-191-2017.
Ploton, P., Mortier, F., Réjou-Méchain, M., Barbier, N., Picard, N., Rossi, V., Dormann, C., Cornu, G., Viennois, G., Bayol, N., Lyapustin, A., Gourlet-Fleury, S., Pélissier, R., 2020. Spatial validation reveals poor predictive performance of large-scale ecological mapping models. Nat. Commun. 11, 4540. https://doi.org/10.1038/s41467-020-18321-y.
Polashenski, C.M., Dibb, J.E., Flanner, M.G., Chen, J.Y., Courville, Z.R., Lai, A.M., Schauer, J.J., Shafer, M.M., Bergin, M., 2015. Neither dust nor black carbon causing apparent albedo decline in Greenland's dry snow zone: implications for MODIS C5 surface reflectance. Geophys. Res. Lett. 42, 9319–9327. https://doi.org/10.1002/2015GL065912.
Qiu, S., Zhu, Z., Shang, R., Crawford, C.J., 2021. Can Landsat 7 preserve its science capability with a drifting orbit? Science of Remote Sensing 4, 100026. https://doi.org/10.1016/J.SRS.2021.100026.
Raup, B., Racoviteanu, A., Khalsa, S.J.S., Helm, C., Armstrong, R., Arnaud, Y., 2007. The GLIMS geospatial glacier database: a new tool for studying glacier change. Global Planet. Change 56, 101–110. https://doi.org/10.1016/j.gloplacha.2006.07.018.
Rienecker, M.M., Suarez, M.J., Gelaro, R., Todling, R., Bacmeister, J., Liu, E., Bosilovich, M.G., Schubert, S.D., Takacs, L., Kim, G.K., Bloom, S., Chen, J., Collins, D., Conaty, A., da Silva, A., Gu, W., Joiner, J., Koster, R.D., Lucchesi, R., Molod, A., Owens, T., Pawson, S., Pegion, P., Redder, C.R., Reichle, R., Robertson, F. R., Ruddick, A.G., Sienkiewicz, M., Woollen, J., 2011. MERRA: NASA's Modern-Era Retrospective analysis for research and applications. J. Clim. 24, 3624–3648. https://doi.org/10.1175/JCLI-D-11-00015.1.
Riggs, G., Hall, D.K., 2020. Continuity of MODIS and VIIRS snow cover extent data products for development of an earth science data record. Rem. Sens. 12, 3781. https://doi.org/10.3390/rs12223781.
Roy, D.P., Borak, J.S., Devadiga, S., Wolfe, R.E., Zheng, M., Descloitres, J., 2002. The MODIS Land product quality assessment approach. Rem. Sens. Environ. 83, 62–76. https://doi.org/10.1016/S0034-4257(02)00087-1.
Roy, D.P., Kovalskyy, V., Zhang, H., Vermote, E., Yan, L., Kumar, S., Egorov, A., 2016. Characterization of Landsat-7 to Landsat-8 reflective wavelength and normalized difference vegetation index continuity. Rem. Sens. Environ. 185, 57–70. https://doi.org/10.1016/j.rse.2015.12.024.
Roy, D.P., Li, Z., Zhang, H.K., Huang, H., 2020. A conterminous United States analysis of the impact of Landsat 5 orbit drift on the temporal consistency of Landsat 5 Thematic Mapper data. Rem. Sens. Environ. 240, 111701 https://doi.org/10.1016/J.RSE.2020.111701.
Ryan, J.C., Hubbard, A., Irvine-Fynn, T.D., Doyle, S.H., Cook, J.M., Stibal, M., Box, J.E., 2017. How robust are in situ observations for validating satellite-derived albedo over the dark zone of the Greenland Ice Sheet? Geophys. Res. Lett. 44, 6218–6225. https://doi.org/10.1002/2017GL073661.
Ryan, J.C., Hubbard, A., Stibal, M., Irvine-Fynn, T.D., Cook, J., Smith, L.C., Cameron, K., Box, J., 2018. Dark zone of the Greenland Ice Sheet controlled by distributed biologically-active impurities. Nat. Commun. 9, 1065. https://doi.org/10.1038/s41467-018-03353-2.
Ryan, J.C., Smith, L.C., van As, D., Cooley, S.W., Cooper, M.G., Pitcher, L.H., Hubbard, A., 2019. Greenland Ice Sheet surface melt amplified by snowline migration and bare ice exposure. Sci. Adv. 5 https://doi.org/10.1126/sciadv.aav3738.
Schaaf, C.B., Gao, F., Strahler, A.H., Lucht, W., Li, X., Tsang, T., Strugnell, N.C., Zhang, X., Jin, Y., Muller, J.P., Lewis, P., Barnsley, M., Hobson, P., Disney, M., Roberts, G., Dunderdale, M., Doll, C., D'Entremont, R.P., Hu, B., Liang, S., Privette, J.L., Roy, D., 2002. First operational BRDF, albedo nadir reflectance products from MODIS. Rem. Sens. Environ. 83, 135–148. https://doi.org/10.1016/S0034-4257(02)00091-3.
Schaaf, C.B., Wang, Z., Strahler, A.H., 2011a. Commentary on Wang and Zender—MODIS snow albedo bias at high solar zenith angles relative to theory and to in situ observations in Greenland. Rem. Sens. Environ. 115, 1296–1300. https://doi.org/10.1016/j.rse.2011.01.002.
Schaaf, C.L.B., Liu, J., Gao, F., Strahler, A.H., 2011b. MODIS albedo and reflectance anisotropy products from Aqua and Terra. Land Remote Sensing and Global Environmental Change: NASA's Earth Observing System and the Science of ASTER and MODIS 11, 549–561.

Schmit, T.J., Griffith, P., Gunshor, M.M., Daniels, J.M., Goodman, S.J., Lebair, W.J., 2017. A closer look at the ABI on the GOES-R series. Bull. Am. Meteorol. Soc. 98, 681–698. https://doi.org/10.1175/BAMS-D-15-00230.1.

Shimada, R., Takeuchi, N., Aoki, T., 2016. Inter-annual and geographical variations in the extent of bare ice and dark ice on the Greenland ice sheet derived from MODIS satellite images. Front. Earth Sci. 4 https://doi.org/10.3389/feart.2016.00043.

Shupe, M.D., Walden, V.P., Eloranta, E., Uttal, T., Campbell, J.R., Starkweather, S.M., Shiobara, M., 2011. Clouds at arctic atmospheric observatories. Part I: occurrence and macrophysical properties. J. Appl. Meteorol. Climatol. 50, 626–644. https://doi.org/10.1175/2010JAMC2467.1.

Sobrino, J.A., Julien, Y., Atitar, M., Nerry, F., 2008. NOAA-AVHRR orbital drift correction from solar zenithal angle data. IEEE Trans. Geosci. Rem. Sens. 46, 4014–4019. https://doi.org/10.1109/TGRS.2008.2000798.

Steffen, K., Box, J., 2001. Surface climatology of the Greenland ice sheet: Greenland climate network 1995-1999. J. Geophys. Res. Atmos. 106, 33951–33964. https://doi.org/10.1029/2001JD900161.

Steffen, K., Box, J.E., Abdalati, W., 1996. Greenland climate network: GC-Net. US Army. Cold Regions Reattach and Engineering (CRREL), CRREL Special Report 98–103.

Steger, C.R., Reijmer, C.H., van den Broeke, M.R., 2017. The modelled liquid water balance of the Greenland Ice Sheet. Cryosphere 11, 2507–2526. https://doi.org/10.5194/tc-11-2507-2017.

Stroeve, J.C., Box, J.E., Gao, F., Liang, S., Nolin, A., Schaaf, C., 2005. Accuracy assessment of the MODIS 16-day albedo product for snow: comparisons with Greenland in situ measurements. Rem. Sens. Environ. 94, 46–60. https://doi.org/10.1016/j.rse.2004.09.001.

Stroeve, J.C., Box, J.E., Haran, T., 2006. Evaluation of the MODIS (MOD10A1) daily snow albedo product over the Greenland ice sheet. Rem. Sens. Environ. 105, 155–171. https://doi.org/10.1016/J.RSE.2006.06.009.

Stroeve, J., Box, J.E., Wang, Z., Schaaf, C., Barrett, A., 2013. Re-evaluation of MODIS MCD43 Greenland albedo accuracy and trends. Rem. Sens. Environ. 138, 199–214. https://doi.org/10.1016/j.rse.2013.07.023.

Tang, X., Bullock, E.L., Olofsson, P., Woodcock, C.E., 2020. Can VIIRS continue the legacy of MODIS for near real-time monitoring of tropical forest disturbance? Rem. Sens. Environ. 249, 112024 https://doi.org/10.1016/j.rse.2020.112024.

Tedstone, A.J., Bamber, J.L., Cook, J.M., Williamson, C.J., Fettweis, X., Hodson, A.J., Tranter, M., 2017. Dark ice dynamics of the south-west Greenland Ice Sheet. Cryosphere 11, 2491–2506. https://doi.org/10.5194/tc-11-2491-2017.

Tedstone, A.J., Cook, J.M., Williamson, C.J., Hofer, S., McCutcheon, J., Irvine-Fynn, T., Gribbin, T., Tranter, M., 2020. Algal growth and weathering crust state drive variability in western Greenland Ice Sheet ice albedo. Cryosphere 14, 521–538. https://doi.org/10.5194/tc-14-521-2020.

Thyng, K., Greene, C., Hetland, R., Zimmerle, H., DiMarco, S., 2016. True colors of oceanography: guidelines for effective and accurate colormap selection. Oceanography 29, 9–13. https://doi.org/10.5670/oceanog.2016.66.

Tian, F., Fensholt, R., Verbesselt, J., Grogan, K., Horion, S., Wang, Y., 2015. Evaluating temporal consistency of long-term global NDVI datasets for trend analysis. Rem. Sens. Environ. 163, 326–340. https://doi.org/10.1016/j.rse.2015.03.031.

Van As, D., Fausto, R.S., 2011. Programme for Monitoring of the Greenland Ice Sheet (PROMICE): first temperature and ablation records. Geol. Surv. Den. Greenl. Bull. 23, 73–76. https://doi.org/10.34194/geusb.v23.4876.

Van As, D., Broeke, M.v.d., Reijmer, C., Wal, R.v.d., 2005. The summer surface energy balance of the high antarctic plateau. Boundary-Layer Meteorol. 115, 289–317. https://doi.org/10.1007/s10546-004-4631-1.

Van As, D., Fausto, R.S., Colgan, W.T., Box, J.E., PROMICE project team, 2013. Darkening of the Greenland ice sheet due to the melt albedo feedback observed at PROMICE weather stations. Geol. Surv. Den. Greenl. Bull. 28, 69–72. https://doi.org/10.34194/geusb.v28.4728.

van As, D., Bech Mikkelsen, A., Holtegaard Nielsen, M., Box, J.E., Claesson Liljedahl, L., Lindbäck, K., Pitcher, L., Hasholt, B., 2017. Hypsometric amplification and routing moderation of Greenland ice sheet meltwater release. Cryosphere 11, 1371–1386. https://doi.org/10.5194/tc-11-1371-2017.

Wang, S., Tedesco, M., Alexander, P., Xu, M., Fettweis, X., 2020. Quantifying spatiotemporal variability of glacier algal blooms and the impact on surface albedo in southwestern Greenland. Cryosphere 14, 2687–2713. https://doi.org/10.5194/tc-14-2687-2020.

Wehrlé, A., Box, J.E., Niwano, M., Anesio, A.M., Fausto, R.S., 2021. Greenland bare-ice albedo from PROMICE automatic weather station measurements and Sentinel-3 satellite observations. GEUS Bulletin 47. https://doi.org/10.34194/geusb.v47.5284.

Williamson, C.J., Cook, J., Tedstone, A., Yallop, M., McCutcheon, J., Poniecka, E., Campbell, D., Irvine-Fynn, T., McQuaid, J., Tranter, M., Perkins, R., Anesio, A., 2020. Algal photophysiology drives darkening and melt of the Greenland Ice Sheet. Proc. Natl. Acad. Sci. USA 117, 5694–5705. https://doi.org/10.1073/pnas.1918412117.

Wright, P., Bergin, M., Dibb, J., Lefer, B., Domine, F., Carman, T., Carmagnola, C., Dumont, M., Courville, Z., Schaaf, C., Wang, Z., 2014. Comparing MODIS daily snow albedo to spectral albedo field measurements in Central Greenland. Rem. Sens. Environ. 140, 118–129. https://doi.org/10.1016/J.RSE.2013.08.044.

Wu, Q., 2020. geemap: a Python package for interactive mapping with Google Earth Engine. J. Open Source Softw. 5, 2305. https://doi.org/10.21105/joss.02305.

Wu, Q., Lane, C.R., Li, X., Zhao, K., Zhou, Y., Clinton, N., DeVries, B., Golden, H.E., Lang, M.W., 2019. Integrating LiDAR data and multi-temporal aerial imagery to map wetland inundation dynamics using Google Earth Engine. Rem. Sens. Environ. 228, 1–13. https://doi.org/10.1016/j.rse.2019.04.015.

Xiao, Y., Ke, C.Q., Fan, Y., Shen, X., Cai, Y., 2022. Estimating glacier mass balance in high mountain asia based on moderate resolution imaging spectroradiometer retrieved surface albedo from 2000 to 2020. Int. J. Climatol. https://doi.org/10.1002/JOC.7873.

Xiong, Xiaoxiong, Wu, Aisheng, Wenny, B.N., Madhavan, S., Wang, Zhipeng, Li, Yonghong, Chen, Na, Barnes, W., Salomonson, V., 2015. Terra and aqua MODIS thermal emissive bands on-orbit calibration and performance. IEEE Trans. Geosci. Rem. Sens. 53, 5709–5721. https://doi.org/10.1109/TGRS.2015.2428198.

Xiong, X., Angal, A., Chang, T., Aldoretta, E., Geng, X., Link, D., Sun, J., Twedt, K., Wu, A., 2023. Aqua MODIS: 20 years of on-orbit calibration and performance. J. Appl. Remote Sens. 17, 037501 https://doi.org/10.1117/1.JRS.17.037501.

Zhang, H., Roy, D.P., 2016. Landsat 5 Thematic Mapper reflectance and NDVI 27-year time series inconsistencies due to satellite orbit change. Rem. Sens. Environ. 186, 217–233. https://doi.org/10.1016/j.rse.2016.08.022.

Zhang, J., Shang, R., Rittenhouse, C., Witharana, C., Zhu, Z., 2021. Evaluating the impacts of models, data density and irregularity on reconstructing and forecasting dense Landsat time series. Science of Remote Sensing 4, 100023. https://doi.org/10.1016/j.srs.2021.100023.

Zhu, Z., Woodcock, C.E., 2012. Object-based cloud and cloud shadow detection in Landsat imagery. Rem. Sens. Environ. 118, 83–94. https://doi.org/10.1016/j.rse.2011.10.028.

Zhu, Z., Wang, S., Woodcock, C.E., 2015. Improvement and expansion of the Fmask algorithm: cloud, cloud shadow, and snow detection for Landsats 4–7, 8, and Sentinel 2 images. Rem. Sens. Environ. 159, 269–277. https://doi.org/10.1016/j.rse.2014.12.014.